Pergamon

SCIENCE DIRECT®

Bioorganic & Medicinal Chemistry 11 (2003) 3133–3140

BIOORGANIC & MEDICINAL CHEMISTRY

Modified Glycopeptides Related to Cell Wall Peptidoglycan: Conformational Studies by NMR and Molecular Modelling

Krisztina Fehér,[a] Primož Pristovšek,[b] László Szilágyi,[a,*] Đurdica Ljevaković[c] and Jelka Tomašić[c]

[a]*Department of Organic Chemistry, University of Debrecen, H-4010 Debrecen, Pf. 20, Hungary*
[b]*National Institute of Chemistry, Hajdrihova 19, SI-1001 Ljubljana, POB 660, Slovenia*
[c]*Institute of Immunology, Rockefellerova 2, HR-10 000 Zagreb, POB 266, Croatia*

Received 14 February 2003; accepted 4 April 2003

Abstract—Polymeric peptidoglycans of bacterial cell walls, and smaller glycopeptides derived from them, exhibit versatile biological activities including immunomodulating properties. Peptidoglycan monomer (PGM) was isolated from *Brevibacterium divaricatum* and novel lipophilic derivatives of PGM bearing either (adamantyl-1-yl)-acetyl or Boc-Tyr substituents (Ad-PGM and BocTyr-PGM respectively) have recently been synthesized. We have obtained full assignments of the ^{1}H and ^{13}C spectra, using 2D NMR techniques, for all three compounds in DMSO solutions. NOESY/ROESY experiments have provided interproton distance restraints that were used in distance geometry modelling calculations to derive conformational preferences for each of these molecules. These data were supplemented with information available from chemical shifts, temperature dependence of amide proton shifts and proton–proton scalar couplings. Analysis of the results suggest that the lipophilic substituents attached to the Dap^{3}-ε amino group of the parent PGM molecule introduce changes to the conformational preferences of the peptide moiety. In PGM electrostatic interactions between charged end groups apparently promote folded conformations with participation of the long Dap side chain. Derivatives wherein such interactions are suppressed by acylation of the Dap^{3}-ε amino group are characterized by more extended conformations of the peptide chain. The new synthetic derivatives exhibit biological properties similar to those of the parent PGM. This may indicate that peripheral parts of the peptide chain such as the C-terminal and end groups of the long Dap side chain do not significantly contribute to the binding to receptors or enzymes participating in the biochemical interactions referred to above.

Introduction

Peptidoglycan are ubiquitous constituents of bacterial cell walls responsible for the physical integrity of bacteria. They are composed of glycan chains which are built of β-1,4-linked *N*-acetyl-D-glucosamine (GlcNAc) and *N*-acetylmuramic acid (MurNAc) residues and peptide units that consist of alternating L- and D-amino acids. The glycan chains are mostly linked through relatively short-chain pepetides. Peptidoglycan fragments exhibit various biological activities that depend upon the size and composition of the peptidoglycan fragments.[1] One of the most prominent and also well documented activity of peptidoglycans is the effect on the mammalian immune system. Low molecular weight peptidoglycan fragments, either obtained from natural sources or prepared synthetically, are mostly devoid of the toxic properties characteristic for large peptidoglycans, but still retain marked immunomodulating activity.[2–4]

Our studies concern the low molecular weight peptidoglycan monomer (PGM, **1**) which is the repeating unit of the cell wall peptidoglycan from *Brevibacterium divaricatum*. PGM was obtained after lysozyme hydrolysis of un-crosslinked peptidoglycan polymer isolated from the culture fluid of penicillin treated bacteria.[5] This disaccharide pentapeptide is water soluble, nontoxic and non pyrogenic and has the chemically well defined structure: D-GlcNAc-β(1→4)-D-MurNAc-L-Ala-D-*iso*Gln-*meso*Dap(εNH$_2$)-D-Ala-D-Ala (Scheme 1).[5,6]

In our earlier studies we have shown that PGM possesses marked immunostimulating activity and could therefore be used as an adjuvant with various antigens.[7,8]

*Corresponding author. Tel.: +36-52-512900x2589; fax: +36-52-453836; e-mail: lszilagyi@tigris.klte.hu

0968-0896/03/$ - see front matter © 2003 Elsevier Science Ltd. All rights reserved.
doi:10.1016/S0968-0896(03)00244-X

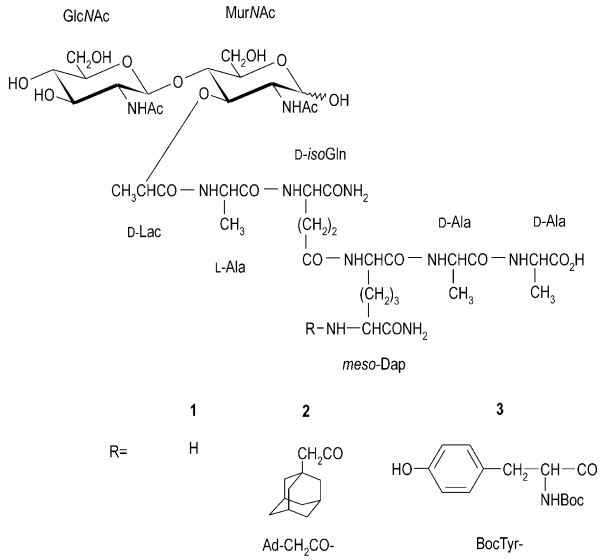

Scheme 1.

Earlier studies of the PGM molecule have also demonstrated that in the preferential conformation in aqueous solution, the ε-amino group of *meso*-diaminopimelic acid (Dap) is exposed[9] and readily available for possible chemical reactions. We have confirmed such observations and synthetized two novel derivatives of PGM, namely, (adamant-1-yl)-CH_2CO-PGM (AdPGM, **2**)[10] and *tert*-butyloxycarbonyl-L-tyrosyl peptidoglycan monomer (Boc-Tyr-PGM, **3**)[11] starting from the unprotected PGM molecule. Both derivatives exhibited immunostimulating activity comparable to the activity of the parent PGM.[10–12] All three compounds are substrates for *N*-acetylmuramyl-L-alanine amidase, as well. The results indicated that the substitution of the free amino group in the PGM molecule with bulky lipophilic substituents did not markedly affect either the immunostimulating activity or the susceptibility towards hydrolysis by *N*-acetylmuramyl-L-alanine amidase.

In view of the similar in vivo behaviour of these three compounds, it was of interest to determine whether these activities are related to similarities in the molecular conformations or, on the other hand, eventual conformational differences may not exert sizeable influence on the biological activity. We have therefore started a comparative study of the conformations of the synthetically modified derivatives **2** and **3** with respect to the unsubstituted PGM, **1**, using NMR spectroscopy and molecular modelling.

The conformational behaviour of peptidoglycan fragments and analogues smaller than PGM has been investigated previously by experimental and computational methods;[13,14] conformational preferences could be identified at the residues close to the glycopeptide junction while no structural preferences were evident for the peptide part following Ala[1]. A detailed conformational study of **1** in *aqueous* solution was carried out using a combined approach by 2D NMR spectroscopy, restrained simulated annealing (SA) and molecular dynamics (MD) calculations;[9] a preliminary investigation in DMSO solution by ^{1}H NMR has been reported previously.[15]

Results and Discussion

The relevant NMR spectral data are summarized in Tables 1 (chemical shifts), 2 (proton–proton couplings and amide temperature coefficients) and 3 (selected NOEs).

Comparison of the data obtained for the parent molecule PGM (**1**) and the derivatives AdPGM (**2**) and BocTyrPGM (**3**) revealed differences in various conformation-related NMR parameters, such as amide ^{1}H chemical shifts (Table 1) and their temperature dependence (Table 2) as well as ^{1}H/^{1}H NOEs (Fig. 1, Table 3). On the other hand, no significant differences were observed in the ^3J(NH,Hα) values (Table 2). The geminal protons of the Dap-$CONH_2$ group display conspicuously large chemical shift non-equivalence (ca. 0.8 ppm) in the unsubstituted parent molecule **1** mainly as a result of a sizeable downfield shift of the resonance for NH_2^E. The downfield shift of the NH_2^Z resonance is much less pronounced with respect to those in the substituted derivatives **2** and **3**, whereas shifts of $CONH_2$ proton resonances of the *i*Gln-residue are very similar in all three compounds and also show reduced shift non-equivalences (see Table 1). The temperature coefficients for all $CONH_2$ protons are in the range of −5 to −7 ppb/K except that for Dap-$CONH_2^E$ in **1** which is approximately twice as large (Table 2). The resonance shift and non-equivalence effects observed for Dap-$CONH_2$ protons in **1** are therefore unlikely to be caused by protection from the solvent through H-bonding; rather, they may be related to steric/conformational differences with respect to **2** and **3** that both bear bulky substituents attached to the end of the Dap side chain. A similar phenomenon is observed for Ala^5-NH in **2**: a relatively large downfield shift, with respect to **1** and **3**, associated with a temperature coefficient of −5.5 ppb/K; the latter indicating appreciable solvent exposure. The same amide proton appears, however, largely protected from solvent in both **1** and **3**, as indicated by the somewhat exceptional, large positive, and low negative, respectively, temperature coefficients, see Table 2. The exceptional temperature coefficient for Ala^5-NH in **1** was also noticed earlier.[15] The conformational preferences at the N-terminal of **2** may therefore be different from those in **1** and **3**.

Conformational differences are reflected in the NOESY cross peak patterns as well. Part of the observed NOEs arise from intraresidue dipolar interactions (*not* listed in Table 3). The majority of the *inter*residue NOE contacts occur between neighbouring residues as evidenced by αN($i,i+1$) and βN($i,i+1$) sequential[16] cross peaks (Table 3). In fact, all possible sequential contacts, either of αN or βN-type,[16] could be observed along the hexapeptide backbone starting with D-Lac; this latter being considered as a ψ-Ala N-terminal residue. Sequential cross peaks like those mentioned are usually observed for small unstructured peptides in aqueous solution.[17]

Table 1. ^{1}H and ^{13}C chemical shift data[a]

	1 (PGM)		**2** (AdPGM)		**3** (BocTyrPGM)	
	δ_{1H}	δ_{13C}	δ_{1H}	δ_{13C}	δ_{1H}	δ_{13C}
β-GlcNAc-1	4.414	100.20	4.428	100.07	4.427	100.07
β-GlcNAc-2	3.404	55.81	3.409	56.03	3.396	56.14
β-GlcNAc-3	3.067[b]	76.53[b]	3.411	75.02	3.396	73.50
β-GlcNAc-4	3.396	73.46	3.074	76.41	3.067	70.84
β-GlcNAc-5	3.057[b]	70.70[b]	3.073	70.85	3.067	76.51
β-GlcNAc-6	3.722	60.99	3.740	61.29	3.715	61.31
β-GlcNAc-6′	3.462	60.99	3.480	61.29	3.462	61.31
β-GlcNAc(CH_3)	1.787	22.73	1.796	22.68	1.792	22.75
β-GlcNAc(NH)	7.808	—	7.768	—	7.821	—
β-GlcNAc(CO)	—	169.27	—		—	169.77
β-GlcNAc-3OH	5.063[c]	—	4.928	—	[f]	—
β-GlcNAc-4OH	5.003[c]	—	4.971	—	[f]	—
β-GlcNAc-6OH	4.343	—	4.239	—	[f]	—
α-MurNAc-1	5.117	89.59	5.119	89.56	5.091	89.71
α-MurNAc-2	3.477	52.38	3.488	53.99	3.502	53.99
α-MurNAc-3	3.401	74.95	3.395	75.03	3.527	71.04
α-MurNAc-4	3.672	75.67	3.683	75.66	3.425[d]	74.96[d]
α-MurNAc-5	3.506	70.93	3.533	71.04	3.670[d]	75.67[d]
α-MurNAc-6	3.602	59.32	3.603	59.38	3.583	59.53
α-MurNAc-6′	3.532	59.32	3.550	59.38	3.539	59.53
α-MurNAc-1OH	6.596	—	6.517	—		—
α-MurNAc(CH_3)	1.804	22.73	1.807	22.68	1.805	22.75
α-MurNAc(NH)	8.454	—	8.395	—	8.423	—
α-MurNAc(CO)	—	169.27	—	169.31	—	169.77
α-MurNAc-6OH	4.610	—	4.570	—		
D-Lac-α	4.462	75.42	4.470	75.38	4.454	75.40
D-Lac-β	1.270	19.17	1.262	19.09	1.253	19.05
D-Lac-CO	—	174.40	—	[e]	—	174.79
L-Ala^1-NH	8.026	—	7.961	—	8.088	—
L-Ala^1-α	4.351	48.14	4.349	48.10	4.329	48.26
L-Ala^1-β	1.241	18.03	1.233	18.05	1.241	18.11
L-Ala^1-CO	—	172.20	—	172.19	—	172.61
D-iGln^2-NH	8.293	—	8.240	—	8.333	—
D-iGln^2-α	4.137	51.93	4.147	51.997	4.115	52.40
D-iGln^2-αCO	—	173.15	—	173.04		
D-iGln^2-NH_2^E	7.355	—	7.289	—	7.359	—
D-iGln^2-NH_2^Z	7.008	—	6.956	—	7.016	—
D-iGln^2-β	1.711	27.35	1.935	27.55	1.996	27.21
D-iGln^2-β′	2.004	27.35	1.709	27.55	1.709	27.21
D-iGln^2-γ,γ′	2.183	31.51	2.144	31.48	2.172	31.38
D-iGln^2-δCO	—	171.67	—	171.67	—	
m-Dap^3-NH	7.969	—	7.998	—	7.857	—
m-Dap^3-α	4.174	53.09	4.161	52.50	4.115	52.40
m-Dap^3-αCO	—	171.11	—	171.14	—	
m-Dap^3-β	1.634	31.63	1.589	31.34	1.533	31.31
m-Dap^3-β′	1.577	31.63	1.471	31.34	1.586	31.31
m-Dap^3-γ	1.413	20.83	1.302	21.64	1.134	21.40
m-Dap^3-γ′	1.350	20.83	1.216	21.64	1.110	21.40
m-Dap^3-δ	1.669	32.20	1.895	27.83	1.615	31.13
m-Dap^3-δ′	1.555	32.20	1.895	27.83	1.373	31.13
m-Dap^3-ε	3.489	53.79	4.133	51.89	4.012	52.04
m-Dap^3-εCO	—	[e]	—	173.80	—	172.96
m-Dap^3-ε$CONH_2^E$	8.107	—	7.248	—	7.355	—
m-Dap^3-ε$CONH_2^Z$	7.287	—	6.912	—	6.938	—
m-Dap^3-εNH	7.878	—	7.647	—	8.073	—
Ad-CH_2-CO	—	—	—	169.66	—	—
Ad-CH_2(α)	—	—	1.879	49.42	—	—
Ad-βC(q)	—	—	—	[e]	—	—
Ad-γCH_2	—	—	1.637	36.24	—	—
Ad-γ′CH_2	—	—	1.573	36.24	—	—
Ad-δCH	—	—	1.898	27.65	—	—
Ad-εCH_2	—	—	1.556	41.79	—	—
L-Tyr-NH	—	—	—	—	7.031	—
Bu′(CH_3)	—	—	—	—	1.316	28.01
L-Tyr-α	—	—	—	—	4.041	56.1
L-Tyr-CO	—	—	—	—	—	171.59
L-Tyr-β	—	—	—	—	2.659	36.28
L-Tyr-β′	—	—	—	—	2.761	36.28
L-Tyr-2,6	—	—	—	—	6.970	129.81
L-Tyr-3,5	—	—	—	—	6.567	114.77
L-Tyr-1	—	—	—	—	—	127.50
L-Tyr-4	—	—	—	—	—	155.97
L-Tyr-4OH	—	—	—	—	6.343	—
D-Ala^4-NH	8.039	—	8.103	—	8.077	—
D-Ala^4-α	4.119	48.58	4.301	47.332	4.124	48.34
D-Ala^4-β	1.212	17.61	1.187	17.91	1.190	17.56
D-Ala^4-CO	—	170.8	—	171.68	—	171.07
D-Ala^5-NH	7.547	—	8.072	—	7.513	—
D-Ala^5-α	3.803	49.15	4.161	47.30	3.731	49.46
D-Ala^5-β	1.192	18.41	1.280	16.76	1.175	18.69
D-Ala^5-CO	—	174.30	—	173.84	—	174.79

[a]For solutions in DMSO-d_6 at 293 K for **1** and at 300 K for **2** and **3**. Chemical shifts are in ppm and referenced to the solvent signal (δ_{1H} = 2.500 ppm, δ_{13C} = 39.95 ppm). $CONH_2^Z$ and $CONH_2^E$ refer to one of the amide protons in *Z* or *E* position with respect to the C=O oxygen, respectively.
[b]Assignment for β-GlcNAc-3 and β-GlcNAc-5 can be interchanged.
[c]Assignment for β-GlcNAc-3OH and β-GlcNAc-4OH can be interchanged.
[d]Assignment for MurNAc-H4 and MurNAc-H5 can be interchanged.
[e]Cannot be determined due to missing crosspeak in HMBC and overlap in the 1D ^{13}C spectra.
[f]Cannot be determined due to missing crosspeak in homonuclear correlation spectra.

On the other hand, NOEs between the carbohydrate and peptide moieties (NOEs #2-20, Table 3) are indicative of less conformational freedom at the N-terminal part of the peptide chain. Strong interglycosidic NOEs (#1) were detected between GlcNAc-H1 and MurNAc-H4 in all three molecules investigated (Table 3).

Inspection of the amide regions in the NOESY maps for **1**, **2** and **3** (Fig. 1) reveals characteristic differences especially with regard to the long-range NOEs (Table 3). Of the three compounds **1** clearly features the largest number of long-range NOEs, several indicating contacts between the MurNAc (especially the *N*-acetyl methyl and MurNAc-2,3 protons) and the N-terminal peptide residues. The number of such contacts is reduced in **2** whereas practically none is observed in **3** (see, Fig. 3 and Table 3). Long-range NOEs involving any of the adamantyl ring protons are conspicuously missing in **2**. On the other hand, Tyr aromatic protons display some contacts with the C-terminal residues of the peptide moiety (such as #33, 36 and 42, see, Table 3 and Fig. 3).

The structures resulting from distance geometry calculations were divided in clusters of conformations (Fig. 2) according to selected main chain dihedral angle values (see Experimental), and the most populated cluster with low energy was chosen to represent the preferred conformations. Selected structures from the representative clusters are shown with an identical orientation of the two sugar units for each of the molecules in Figure 3. In Table 4 some statistical data are shown regarding the main chain dihedral angle values used for clustering of conformations, and a comparison with the values for **1** from an explicit water simulation[9] is given. Additionally, the calculated values for selected $^3J_{HN,\alpha}$ coupling constants[16,18] are shown for the representative clusters. The latter are reasonably similar to

Table 2. ^{1}H NMR coupling constants and amide temperature coefficients for **1** (PGM), **2** (Ad-PGM) and **3** (BocTyr-PGM)

Residue	^3J(NH,Hα) (Hz)			Δδ/ΔT (−ppb/K)		
	1	**2**	**3**	**1**	**2**	**3**
β-GlcNAc	8.4 (8.4[a]; 9.6[b])	7.6	8.4	5.4 (11.8[b])	4.5	4.4
α-MurNAc	5.7 (7.9[a]; 7.5[b])	5.7	6.1	11.7 (4.3[b])	11.4	10.0
L-Ala^1	∼7 (8.0[a]; 5.4[b])	7.0	n.a.	∼10 (13.8[b])	7.0	∼6
D-*i*Gln^2	8.1 (8.0[a]; 7.8[b])	8.1	7.0	7.8 (13.7[b])	6.7	4.8
m-Dap^3 (α)	7.5 (7.6[a]; 6.8[b])	7.6	7.8	***0.4*** (10.5[b])	5.9	5.2
D-Ala^4	∼7 (7.2[a]; 6.8[b])	8.1	n.a.	∼10 (10.4[b])	7.5	∼6
D-Ala^5	6.4 (6.4[a]; 6.9[b])	7.2	∼5	***−8.1*** (12.5[b])	5.5	***2.2***
m-Dap^3 (ε)	—	8.1	n.a.	—	6.1	∼6
D-*i*Gln-CONH$_2^E$				6.4	5.3	∼5
D-*i*Gln-CONH$_2^Z$				5.4	4.9	∼7
m-Dap-CONH$_2^E$				∼14	5.9	∼5
m-Dap-CONH$_2^Z$				4.6	5.3	5.4

[a]In ***DMSO***, from ref 15.
[b]In ***H_2O***: from ref 9.

the experimental values (Table 2). The orientation of the Lac-Ala^1-*i*Gln^2 moiety is similar, though not identical, for **1** and **2**, but differs more strongly with **3**. With **1** the orientation of the N-terminal peptide domain relative to the disaccharide moiety is characterized by NOEs from the *i*Gln^2 to MurNAc (#6, 11, 17 and 18 in Table 3, Figs 1 and 3) while with **2** the Lac moiety displays a different orientation that leads to an interesting NOE contact with MurNAc-H2 (#3 in Table 3, Fig. 3). On the other hand, **3** displays unique contacts of the MurNAc to Lac as well as to Ala^4 (#19 and 14 in Table 3, Fig. 3).

The structure of **1** can be used for an explanation of the unusual *positive* temperature coefficient of the Ala^5-NH chemical shift (Table 2). The latter could be caused by the protection of Ala^5-NH from solvent by the side chain of Dap^3 that is attracted towards the negatively charged Ala^5-C-terminus by the positively charged Dap^3-εNH$_3^+$ group. Such a charged group is absent in **2** and **3**, where the respective temperature coefficients are in the negative range. Additionally, **1** shows long-range NOEs from the *i*Gln^2 to the sugar moiety (see above); the resulting conformations partially protect Dap-NH from solvent and may lower its temperature dependence (Table 2) although the exact mechanism is not evident from the NOE pattern. The preferred conformation of **1** in DMSO as determined in the present study is rather different from the average structure of **1** that has been calculated in water.[9] The significant differences obtained for the torsion angles of the peptide residues proximal to MurNAc (Table 4) are also reflected in the NOE patterns: the *i*Gln^2 to MurNAc NOEs observed for **1** in DMSO (see above) are missing in H_2O solution.[9] More importantly, long-range NOEs seen between Ala^5-NH and Dap^3 side-chain protons (#34, 35 and 37, see below) for **1** in DMSO are absent in H_2O.[9] **2** is devoid of any remarkable NOEs, including those involving the adamantyl moiety, or anomalous amide chemical shift temperature dependences. Correspondingly, the calculated structures are also the least constrained by distance restraints of the three molecules (Fig. 2).

BocTyrPGM (**3**), however, displays a network of hydrophobic interactions also involving the Bu^t of Boc and aromatic protons, exemplified by the NOEs MurNAc(CH$_3$) to Ala^4-β (#14 in Table 3 and Fig. 3), Tyr-3,5 to Ala^4-β (#42 in Table 3, Figs 1 and 3), and Tyr-3,5 to Bu^t(Boc) (#43 in Table 3). The resulting structures fully expose Dap-NH but partially hide the Ala^5-NH from solvent in partial agreement with the temperature coefficients (Table 2). The high-field shift of Ala^5-NH in **1** and **3** relative to **2** seems to be connected with its protection from solvent. The low-field shift of the Dap^3-NH$_2^E$ and -NH$_2^Z$ protons in **1** relative to **2** and **3** (cf. Table 1) is most probably caused by the proximity of the Dap^3-εNH$_3^+$ amino group.

Table 3. NOESY/ROESY cross peak intensities for **1** (PGM), **2** (Ad-PGM) and **3** (BocTyr-PGM)[a,b,c]

	Proton1	Proton2	**1**[d]	**2**[d]	**3**[e]
1	GlcNAc-1	MurNAc-4	s	s	s
2	GlcNAc-3	D-Lac-β	—	—	w[i]
3	MurNAc-2	D-Lac-α	—	m	—
4	MurNAc-2	D-Lac-β	m	s	m
5	MurNAc-2	L-Ala^1-NH	m	m	w
6	MurNAc-2	D-*i*Gln^2-NH	w	—	—
7	MurNAc-NH	D-Lac-α	s	s	m
8	MurNAc-NH	D-Lac-β	s	m	w
9	MurNAc(CH$_3$)	L-Ala^1-NH	w	w	—
10	MurNAc(CH$_3$)	L-Ala^1-β	—	—	w
11	MurNAc(CH$_3$)	D-*i*Gln^2-NH	w	—	—
12	MurNAc(CH$_3$)	D-*i*Gln^2-CONH$_2^E$	w	w	w[g]
13	MurNAc(CH$_3$)	D-*i*Gln^2-CONH$_2^Z$	w	w	—
14	MurNAc(CH$_3$)	D-Ala^4-β	—	—	w
15	MurNAc-3	D-Lac-β	m	m	w
16	MurNAc-3	L-Ala^1-NH	m	w	—
17	MurNAc-3	D-*i*Gln^2-NH	w	—	—
18	MurNAc-3	D-*i*Gln^2-CONH$_2^E$	w	—	—
19	MurNAc-4	D-Lac-β	—	—	w
20	MurNAc-4	L-Ala^1-NH	w	w	—
21	D-Lac-α	L-Ala^1-NH	s	s	s
22	D-Lac-β	L-Ala^1-NH	s	s	s[f]
23	D-Lac-β	D-*i*Gln^2-CONH$_2^E$	w	—	w[f]
24	L-Ala^1-α	D-*i*Gln^2-NH	s	s	s
25	L-Ala^1-α	D-*i*Gln^2-CONH$_2^E$	w	w	w
26	L-Ala^1-β	D-*i*Gln^2-NH	s	s	s
27	L-Ala^1-β	D-*i*Gln^2-γ,γ′	—	—	w
28	L-Ala^1-β	D-iGln^2-CONH$_2^E$		w	w[f]
29	D-*i*Gln^2-β,β′	*m*-Dap^3-αNH	m	w	w
30	D-*i*Gln^2-γ,γ′	*m*-Dap^3-αNH	s	s	s
31	*m*-Dap^3-α	D-Ala^4-NH	s	s	s[g]
32	*m*-Dap^3-β,β′	D-Ala^4-NH	m	m	m
33	*m*-Dap^3-β,β′	L-Tyr-3,5	[h]	[h]	w
34	*m*-Dap^3-β,β′	D-Ala^5-NH	w	—	w
35	*m*-Dap^3-γ,γ′	D-Ala^5-NH	m	—	—
36	*m*-Dap^3-γγ′	L-Tyr-3,5	[h]	[h]	w
37	*m*-Dap^3-ε	D-Ala^5-NH	w	—	—
38	*m*-Dap^3-εNH	(Ad)-CH$_2$-(CO)	[h]	s	[h]
39	*m*-Dap^3-εNH	L-Tyr-α	[h]	[h]	s
40	*m*-Dap^3-εNH	L-Tyr-β,β′	[h]	[h]	m
41	D-Ala^4-α	D-Ala^5-NH	s	s	s
42	D-Ala^4-β	L-Tyr-3,5	[h]	[h]	w
43	Boc-Bu^t	L-Tyr-3,5	[h]	[h]	w

[a]NOEs only for the dominant isomer with the reducing MurNAc moiety in α-anomeric form.
[b]Interresidual cross peaks are only listed. The actual number of distance restraints used for the calculations was larger see text.
[c]CONH$_2^Z$ and CONH$_2^E$ refer to one of the amide protons in *Z* or *E* position with respect to the C=O oxygen, respectively.
[d]Determined from NOESY spectra recorded at 300 K.
[e]Determined from ROESY spectra recorded at 300 K.
[f]Ambiguous: L-Ala^1-β and D-Lac-β overlap.
[g]Ambiguous: MurNAc(CH$_3$) and GlcNAc(CH$_3$) overlap.
[h]Does not apply.
[i]Ambiguous: GlcNAc-3 and GlcNAc-5 overlap.

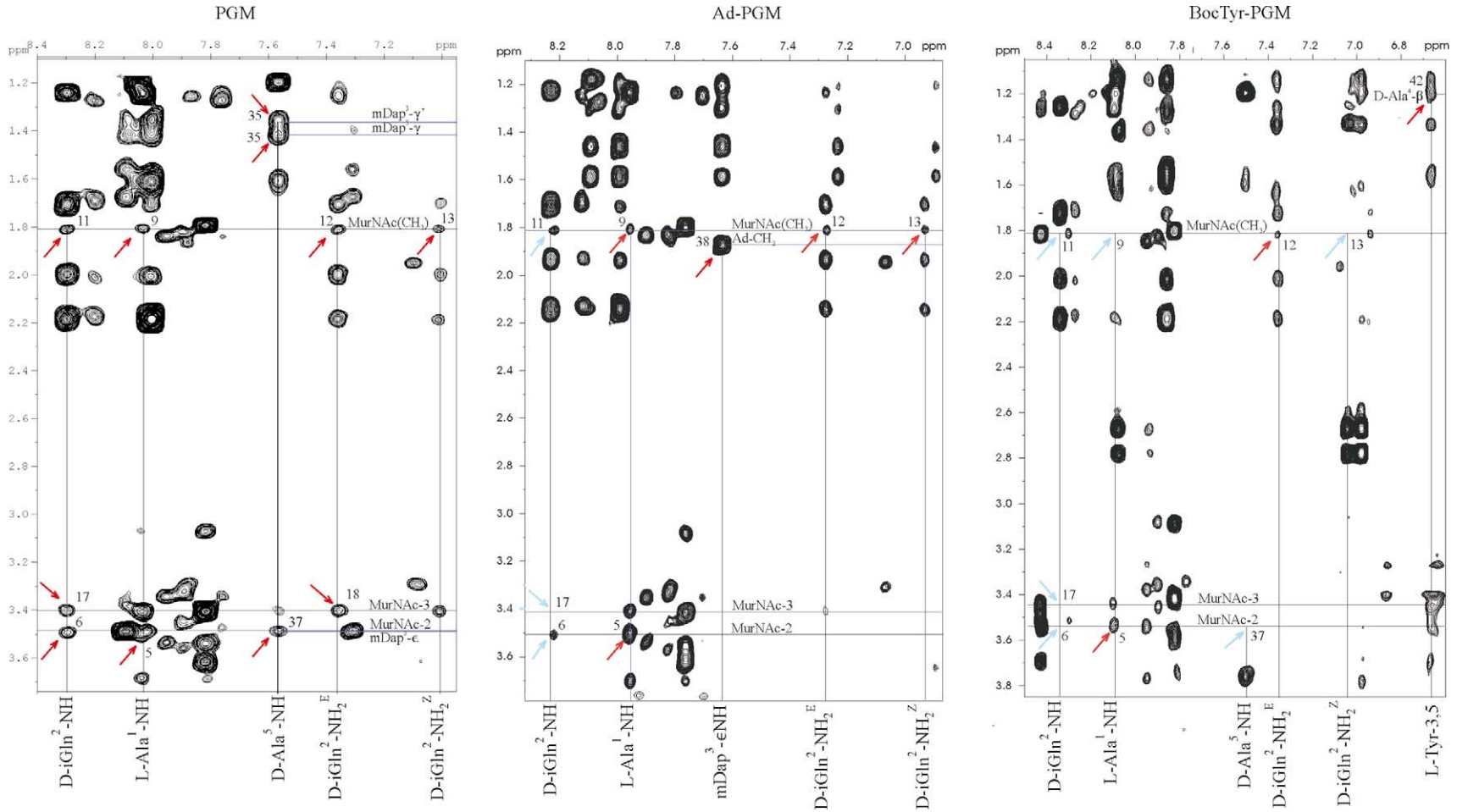

Figure 1. Partial NOE maps of **1** (PGM, left), **2** (Ad-PGM, centre) and **3** (BocTyr-PGM, right) emphasizing the presence (arrows in red) or absence (arrows in blue) of characteristic long-range cross peaks. Cross peaks are labelled using peak numbers in Table 3.

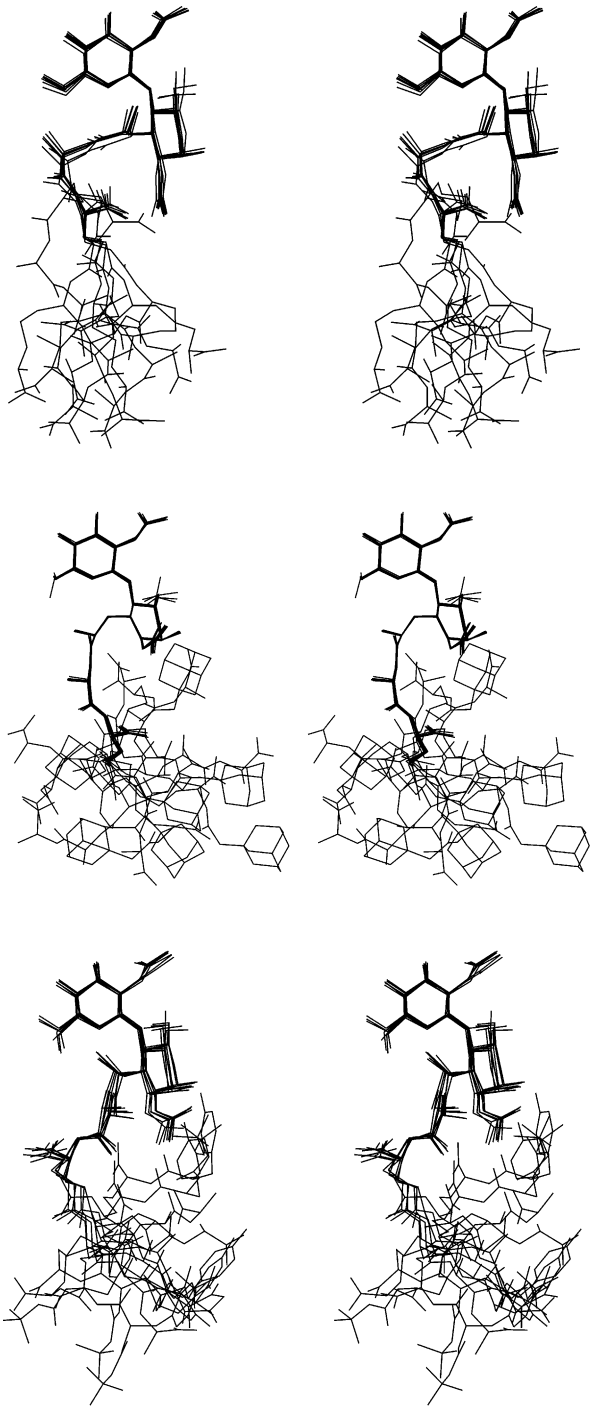

Figure 2. Stereoviews of nine structures from the most populated clusters with low energy for **1** (PGM, top), **2** (Ad-PGM, middle) and **3** (BocTyr-PGM, bottom) superposed at the heavy atoms of the GlcNAc, MurNAc, D-Lac, L-Ala[1] and D-*i*Gln[2] moieties. The RMSD values (calculated at the heavy atoms of GlcNAc, MurNAc, Lac, Ala[1] and *i*Gln[2]) of the ensembles are 1.10, 0.80 and 0.85 Å for **1**, **2** and **3**, respectively.

The results shown above suggest that the lipophilic substituents attached to the Dap[3]-εNH_2 amino group of the parent PGM molecule introduce changes in the conformational preferences of the peptide moiety. In PGM electrostatic interactions between charged end groups (Ala[5]-COO^- and Dap[3]-εNH_3^+) apparently promote folded conformations with participation of the long Dap side chain, as indicated by the unique, long-range NOE contacts between Ala[5]-NH and Dap[3] side-chain protons (#34, 35 and 37 in Table 3, Figs 1 and 3). Derivatives wherein such interactions are suppressed by acylation of the Dap[3]-εNH_2 are characterized by more extended conformations of the peptide chain. The above long range interactions are missing in AdPGM and, conspicuously, no NOEs can be observed involving any of the adamantly ring protons. Of the two acylated derivatives studied AdPGM appears to be less constrained than BocTyrPGM (Fig. 2), the latter being characterized by hydrophobic contacts of the methyl, the aromatic and the Bu^t groups. On the other hand, the absence of long range NOE contacts between Ala[5]-NH and Dap[3] side-chain protons for PGM in H_2O solution (see above) indicates weakened attraction between the charged end groups in that solvent. This may be attributed to the hydration of these charged groups by the more polar water molecules and the ensuing effective shielding from electrostatic attraction between them in H_2O. The conformations of the glycosidic bond in PGM are, on the other hand, similar in DMSO and H_2O (Table 4).

The differences in conformational preferences revealed in solutions for DMSO do not, however, seem to influence the biological activities such as immunostimulation and binding to *N*-acetylmuramyl-L-alanine amidase.[10–12] This may indicate that peripheral parts of the peptide chain such as the C-terminal and end groups of the long Dap side chain do not significantly contribute to the binding to receptors or enzymes, participating in these biochemical interactions, under physiological conditions.

Experimental

Samples

PGM (**1**) was obtained from a penicillin-treated mutant of *B. divaricatum*.[5,19] Derivatives **2** and **3** were synthesized from **1** according to published procedures.[10,11] The NMR samples contained 4–8 mg amounts of material dissolved in 0.5 mL of 99.9% DMSO-d_6.

NMR measurements have been carried out on a Bruker DRX-500 spectrometer using a 5-mm BB probehead equipped with *z*-gradient coil. Spectra were recorded at a temperature where the chemical shift distribution was dispersed optimally in the amide proton region, that is at 300 K for AdPGM and BocTyrPGM and at 293 K for PGM. Amide ^1H chemical shift temperature coefficients have been determined over a temperature range between 293 and 308 K using 5 K increments. Proton and carbon chemical shift scales were calibrated to the DMSO-d_6 solvent signal at 2.500 ppm for ^1H and 39.95 ppm for ^{13}C. The raw datasets typically consisted of 1–2 K×512 complex data points.

NMR assignments

In solution all three compounds exist as equilibrium mixtures of the α- and β-anomeric forms at the reducing MurNAc end of these molecules. Partial ^1H NMR

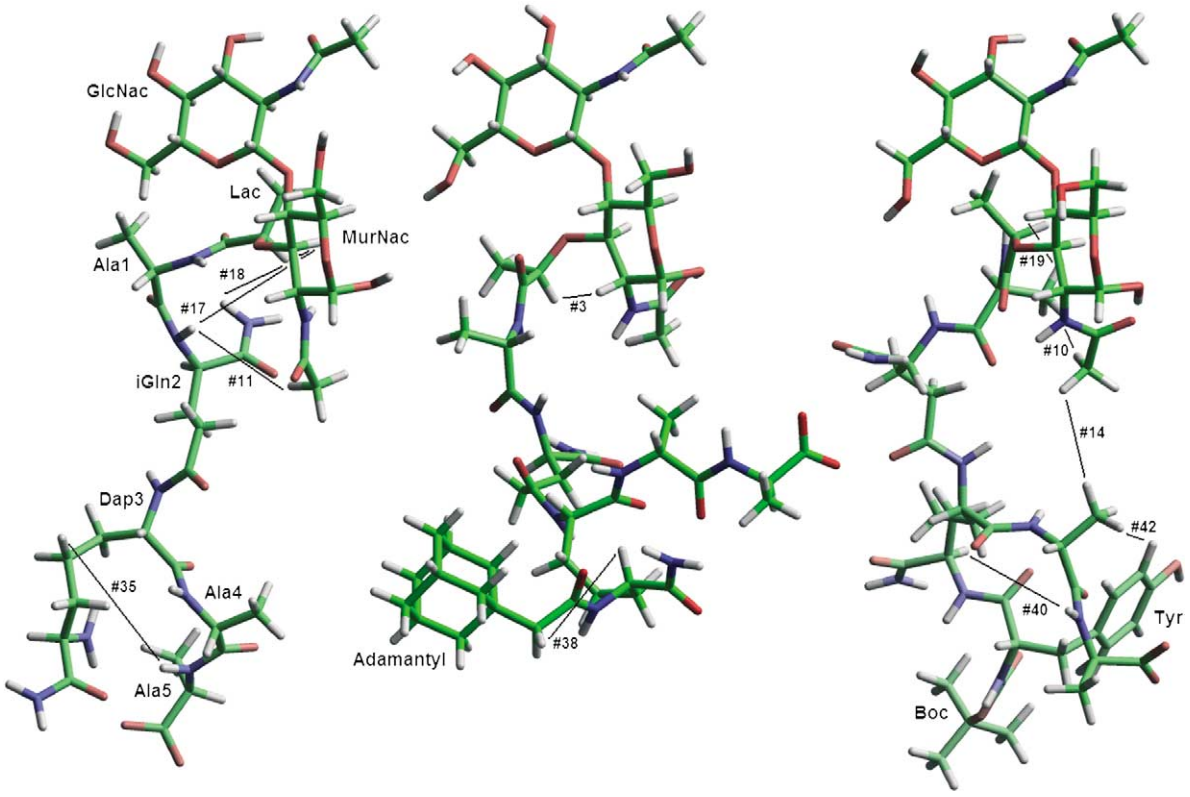

Figure 3. Representative structures for the preferred conformation of **1** (PGM, left) and derivatives **2** (Ad-PGM, centre) and **3** (BocTyr-PGM, right). Selected long-range NOEs are displayed as lines and labelled according to Table 3. An identical orientation of the two sugar moieties was chosen for all three molecules.

Table 4. Average values of selected dihedral angles (in degrees)[a] and ^3J(HN,Hα) coupling constants (in Hz) calculated[b] for the representative clusters of **1** (PGM), **2** (Ad-PGM) and **3** (BocTyr-PGM)

Residue	1[c]	2	3
*i*Gln^2-χ_2	−67 (81)	−64	56
*i*Gln^2-χ_1	−161 (177)	164	131
*i*Gln^2-ψ	−74 (77)	−77	−72
*i*Gln^2-ϕ	80 (123)	76	130
Ala^1-ψ	58 (130)	126	100
Ala^1-ϕ	55 (−160)	175	0
Lac-ψ′	−7 (−166)	−136	−172
Lac-ϕ′	165 (84)	62.8	112
α-MurNAc-ϕ′	121 (−161)	−106	115
β-GlcNAc-ψ	120 (118)	123	121
β-GlcNAc-ϕ′	165 (164)	162	165
^3J(iGln^2-α)	8.5 (n.a.)	7.3	7.7
^3J(Ala^1-α)	6.8 (n.a.)	6.5	6.6
^3J(MurNAc)	5.4 (n.a.)	8.5	8.7
^3J(GlcNAc)	8.7 (n.a.)	8.2	8.6

[a]For the definition of the dihedral angles, see text.
[b]Using Karplus parameters from ref 16.
[c]Values in parentheses are those for **1** calculated for solution in water; from ref 9.

assignments have been reported for the α anomeric form of **1** in DMSO solution[15] whereas tentative ^{13}C assignments were deduced, by comparison with model compounds, for the same in D_2O solution.[20] We have now achieved full assignments of ^{1}H and ^{13}C signals of the major α-anomeric forms, relying on various 2D measurements, for **1**, **2** and **3**. ^{1}H NMR assignments have been based on gradient COSY[21] and 2D TOCSY experiments[22] recorded with different mixing times (50 and 80 ms). The doublet signals of the anomeric protons served as starting points to derive assignments for the disaccharide moiety. Individual side-chain resonances for the peptide part have been identified by characteristic cross peak patterns in the TOCSY maps. For the assignment of some of the sugar ring protons, HSQC-TOCSY measurements[23] were necessary. These assignments have been cross-checked through 1D TOCSY measurements.[24] Three-bond Hα/C=O correlations in the gradient HMBC spectra[25] and Hα/NH sequential cross peaks between two Ala residues in the NOESY maps helped to establish sequential assignments for the three Ala residues. Hε of *m*-Dap exhibited a four-bond coupling to $\varepsilon CONH_2^Z$ in the COSY/TOCSY maps; this was further confirmed by appropriate HMBC cross peaks. HSQC measurements[26] have furnished assignments for protonated carbons whereas ^{13}C HMBC experiments provided identification for the C=O signals. The NMR chemical shift data are shown in Table 1 while Table 2 lists ^3J(NH,Hα) values and temperature dependence of amide NH chemical shifts.

NMR parameters

^{1}H chemical shifts and conformationally important homonuclear coupling constants were extracted from

a resolution enhanced 1D spectrum or, in case of signal overlap, from selective TOCSY experiments. $^1H/^1H$ distance information was obtained using phase sensitive NOESY spectra. ROESY and T-ROESY[27] have also been recorded to crosscheck for peaks resulting from coherent or mixed magnetization transfer. NOE buildup curves were constructed from experiments with mixing times of 50, 100, 150 and 300 ms; values up to 100 ms were found to be in the linear regime. The cross peak intensities were determined by volume integration from the baseplane corrected NOESY or ROESY spectra recorded with 100 ms mixing time.

Computational procedures

The cross-peaks obtained from NOESY and/or ROESY spectra were converted to NOE distance restraints and used in distance geometry calculations followed by energy minimization in the classical force field *cvff*[28] employing the DGII and DISCOVER modules of InsightII (Accelrys Inc., 9685 Scranton Road, San Diego, CA), respectively. The NOE distance restraints were divided in strong, medium and weak with upper limits of 2.6, 3.6 and 5 Å, respectively. The number of distance restraints used for the structure calculations was: 64 for **1**, 67 for **2** and 76 for **3**. Only *inter*-residual experimental contacts are listed in Table 3. For prochiral protons or proton groups a pseduoatom correction was applied.[16] One hundred structures were calculated for each of the molecules and divided in clusters of conformations according to values of the dihedral angles GlcNAc-ϕ', GlcNAc-ψ, MurNAc-ψ', Lac-ϕ', Lac-ψ', Ala^1-ϕ, Ala^1-ψ, *i*Gln^2-ϕ, *i*Gln^2-ψ, *i*Gln^2-χ_1 and *i*Gln^2-χ_2 with a tolerance of 30° [GlcNAc-ϕ', C2-C1-O1-C4(MurNAc); GlcNAc-ψ, C1-O1-C4(MurNAc)-C3(MurNAc); MurNAc-ϕ', C4-C3-O3-Lac-α; Lac-ϕ', C3-O3-Lac-α-Lac-C′; Lac-ψ', O3-Lac-α-Lac-C′-Ala^1-N; the definition of the *i*Gln dihedral angles is used irrespective of the *i*Gln^2-Cγ-Dap^3-N linkage]. The most populated cluster with low energy was chosen to represent the preferred conformations.[29]

Acknowledgements

This research was supported by grants from the National Science Fund of Hungary (OTKA T034515 to L.Sz.), the Hungarian-Slovenian Scientific & Technological Cooperation (S&T) Program and the Ministry of Science and Technology of Croatia (project nr. 021-002). P.P. thanks the Slovenian Ministry for Education, Science and Sport for financial support.

References and Notes

1. Seidl, P. H.; Schleifer, K. H. *Biological Properties of Peptidoglycans*; W. de Gruyter: Berlin, 1986.
2. Ellouz, F.; Adam, A.; Ciorbaru, R.; Lederer, E. *Biochem. Biophys. Res. Commun.* **1974**, *59*, 1317.
3. Azuma, I. *Vaccine* **1992**, *10*, 1000.
4. Stewart-Tull, D. E. S. *Prog. Drug Res.* **1988**, *32*, 305.
5. Keglević, D.; Ladešić, B.; Tomašić, J.; Valinger, Z.; Naumski, R. *Biochim. Biophys. Acta* **1979**, *585*, 273.
6. Tomašić, J.; Sesartić, L.; Martin, S. A.; Valinger, Z.; Ladešić, B. *J. Chromatog.* **1988**, *440*, 405.
7. Tomašić, J.; Hršak, I.; Schrinner, E.; Richmond, M. H.; Seibert, G.; Schwartz, U., Eds.; Surface Structures of Microorganisms and Their Interaction with the Mammalian Host, VCH Ges., 1988; pp 113–121.
8. Tomašić, J.; Hanzl-Dujmović, I.; Špoljar, B.; Vranešić, B.; Šantak, M.; Jovičić, A. *Vaccine* **2000**, *18*, 1236.
9. Matter, H.; Szilágyi, L.; Forgó, P.; Marinić, Ž.; Klaić, B. *J. Am. Chem. Soc.* **1997**, *119*, 2212.
10. Ljevaković, D.; Tomašić, J.; Šporec, V.; Halassy Špoljar, B.; Hanzl-Dujmović, I. *Bioorg. Med. Chem.* **2000**, *8*, 2441.
11. Hršak, I.; Ljevaković, D.; Tomašić, J.; Vranešić, B.; Masihi, N., Ed.; Immunotherapy of Infections, Marcel Dekker, Inc, 1994; pp 249–257.
12. Vranešić, B.; Ljevaković, D.; Tomašić, J.; Ladešić, B. *Clin. Chim. Acta* **1991**, *202*, 23.
13. Pristovšek, P.; Kidrić, J.; Mavri, J.; Hadži, D. *Biopolymers* **1993**, *33*, 1149.
14. Pristovšek, P.; Kidrić, J. *Biopolymers* **1997**, *42*, 659.
15. Klaić, B.; Domenick, R. L. *Carbohydr. Res.* **1990**, *196*.
16. Wüthrich, K. *NMR of Proteins and Nucleic Acids*; John Wiley & Sons: New York, 1986.
17. Dyson, H. J.; Merutka, G.; Waltho, J. P.; Lerner, R. A.; Wright, P. E. *J. Mol. Biol.* **1992**, *226*, 795.
18. Malkin, V. G.; Malkina, O. L.; Casida, M. E.; Salahub, D. R. *J. Am. Chem. Soc.* **1994**, *116*, 5898.
19. Keglević, D.; Ladešić, B.; Hadžija, O.; Tomašić, J.; Valinger, Z.; Pokorny, M.; Naumski, R. *Eur. J. Biochem.* **1974**, *42*, 389.
20. Klaić, B. *Carbohydr. Res.* **1982**, *110*, 320.
21. von Kienlin, M.; Moonen, C. T. W.; van der Toorn, A.; van Zijl, P. C. M. *J. Magn. Reson.* **1991**, *93*, 423.
22. Kövér, K. E.; Uhrín, D.; Hruby, V. J. *J. Magn. Reson.* **1998**, *130*, 162.
23. Kövér, K. E.; Hruby, V. J.; Uhrín, D. *J. Magn. Reson.* **1997**, *129*, 125.
24. Facke, T.; Berger, S. *J. Magn. Reson. Ser. A* **1995**, *113*, 257.
25. Willker, W.; Leibfritz, D.; Kerssebaum, R.; Bermel, W. *Magn. Reson. Chem.* **1993**, *31*, 287.
26. Kay, L. E.; Keifer, P.; Saarinen, T. *J. Am. Chem. Soc.* **1992**, *114*, 10663.
27. Hwang, T.-L.; Shaka, A. J. *J. Magn. Reson. Ser. B* **1993**, *102*, 155.
28. Dauber-Ogusthorpe, P.; Roberts, V. A.; Ogusthorpe, D. J.; Wolff, D. J.; Genest, M.; Hagler, A. T. *Proteins Struct. Funct. Genet.* **1988**, *4*, 31.
29. Pristovšek, P.; Kidrić, J.; Hadži, D. *J. Chem. Inf. Comp. Sci.* **1995**, *35*, 633.